nature energy

ARTICLES

PUBLISHED: 27 JUNE 2016 | ARTICLE NUMBER: 16089 | DOI: 10.1038/NENERGY.2016.89

Fast charge separation in a non-fullerene organic solar cell with a small driving force

Jing Liu[1†], Shangshang Chen[1†], Deping Qian[2], Bhoj Gautam[3], Guofang Yang[1,4], Jingbo Zhao[1], Jonas Bergqvist[2], Fengling Zhang[2], Wei Ma[4], Harald Ade[3], Olle Inganäs[2], Kenan Gundogdu[3*], Feng Gao[2*] and He Yan[1,5*]

Fast and efficient charge separation is essential to achieve high power conversion efficiency in organic solar cells (OSCs). In state-of-the-art OSCs, this is usually achieved by a significant driving force, defined as the offset between the bandgap (E_{gap}) of the donor/acceptor materials and the energy of the charge transfer (CT) state (E_{CT}), which is typically greater than 0.3 eV. The large driving force causes a relatively large voltage loss that hinders performance. Here, we report non-fullerene OSCs that exhibit ultrafast and efficient charge separation despite a negligible driving force, as E_{CT} is nearly identical to E_{gap}. Moreover, the small driving force is found to have minimal detrimental effects on charge transfer dynamics of the OSCs. We demonstrate a non-fullerene OSC with 9.5% efficiency and nearly 90% internal quantum efficiency despite a low voltage loss of 0.61 V. This creates a path towards highly efficient OSCs with a low voltage loss.

Bulk heterojunction (BHJ) OSCs are promising for the realization of low-cost solar energy conversion due to their attractive properties of light weight, mechanical flexibility and roll-to-roll processability method[1–7]. One of the most important factors that limit the efficiency of OSCs is the relatively large voltage loss from the bandgap E_{gap} of the absorber to the open-circuit voltage (V_{oc}) of the cell[8]. For example, the most efficient OSC reported to date has a V_{oc} of 0.77 V for an E_{gap} of 1.65 eV, indicating a voltage loss of 0.88 V (ref. 6). In contrast, state-of-the-art *c*-Si or perovskite cells have voltage losses in the range of 0.40–0.55 V (ref. 8). The large voltage loss in high-efficiency OSCs is due to two main factors. One is the relatively large non-radiative recombination loss in OSCs, evidenced by extremely low electroluminescence quantum efficiency (EQE_{EL}) of OSC blends (typically in the range of 10^{-6}–10^{-8})[9]. The other is the existence of a significant offset between the bandgap of the donor/acceptor materials and the energy of the CT state ($E_{gap} - E_{CT}$)[10–14]. The energy offset is the driving force of charge separation in OSC. Historically, it was believed that a significant driving force is necessary to achieve fast and efficient charge separation in OSCs. There have been several attempts to reduce the driving force and thus the voltage loss in state-of-the-art OSCs[15–23]. Most of these attempts resulted in significantly reduced external quantum efficiency (EQE) and power conversion efficiency (PCE) for the solar cell devices. Among these attempts, the best result was achieved by a polymer named PNOz4T that yield a V_{oc} of 0.96 V and a high efficiency of 8.9%[23]. In that case, the charge separation kinetics was relatively slow (100 ps) and the photoluminescence (PL) quenching was about 66%, which was attributed to large domain size. The existence of a significant driving force in state-of-the-art OSCs creates a problematic trade-off between the V_{oc} and short-circuit current density (J_{sc}) of the OSCs, limiting the maximum achievable efficiency for OSCs.

Therefore, it is important to demonstrate an OSC with a minimal driving force yet can still achieve fast and efficient charge separation. In addition to decreasing the driving force, another way to further increase the V_{oc} is to reduce the non-radiative recombination, which will improve the EQE_{EL} of the solar cells. If both of these (small driving force and high EQE_{EL}) can be achieved, it will be possible to achieve efficient OSCs with a small voltage loss, which then could remove the negative trade-off between V_{oc} and J_{sc}. Lastly, note that fullerene derivatives have been the most dominant choice of acceptor materials for the past 25 years due to their preeminent electron accepting and transporting properties[24,25]. Recently, the field of non-fullerene OSCs has seen a rapid development, with many reports of high-performance small molecular acceptors (SMAs)[23,26–32]. One advantage of non-fullerene OSCs is that it is much more convenient to tune the energy offset between the donor and acceptor, as their energy levels can be readily changed.

Here we report a non-fullerene OSC (based on a novel polymer named P3TEA and a SMA named SF-PDI_2, Fig. 1a) that has a negligible driving force yet exhibits fast and efficient charge separation. The CT state of the P3TEA:SF-PDI_2 blend (blend A) has almost the same energy as the singlet exciton (E_X) of the pure polymer, since the Fourier-transform photocurrent spectroscopy external quantum efficiency (FTPS-EQE) and electroluminescence (EL) spectra of the blend are identical to those of the pure polymer. This translates to a negligible driving force for the blend A-based cells. Transient absorption spectroscopy (TAS) data show that the charge separation dynamics of blend A is ultrafast, with a photoinduced electron transfer half-life of 3 ps. In addition, we show that blend A exhibits a relatively high EQE_{EL} of 0.5×10^{-4},

[1]Department of Chemistry and Energy Institute, The Hong Kong University of Science and Technology, Clear Water Bay, Hong Kong. [2]Department of Physics Chemistry and Biology (IFM), Linköping University, Linköping SE-581 83, Sweden. [3]Department of Physics and Organic and Carbon Electronics Laboratory, North Carolina State University, Raleigh, North Carolina 27695, USA. [4]State Key Laboratory for Mechanical Behavior of Materials, Xi'an Jiaotong University, Xi'an 710049, China. [5]The Hong Kong University of Science and Technology-Shenzhen Research Institute No. 9, Yuexing 1st Road, Hi-tech Park, Nanshan Shenzhen 518057, China. [†]These authors contributed equally to this work. *e-mail: kenan_gundogdu@ncsu.edu; fenga@ifm.liu.se; hyan@ust.hk

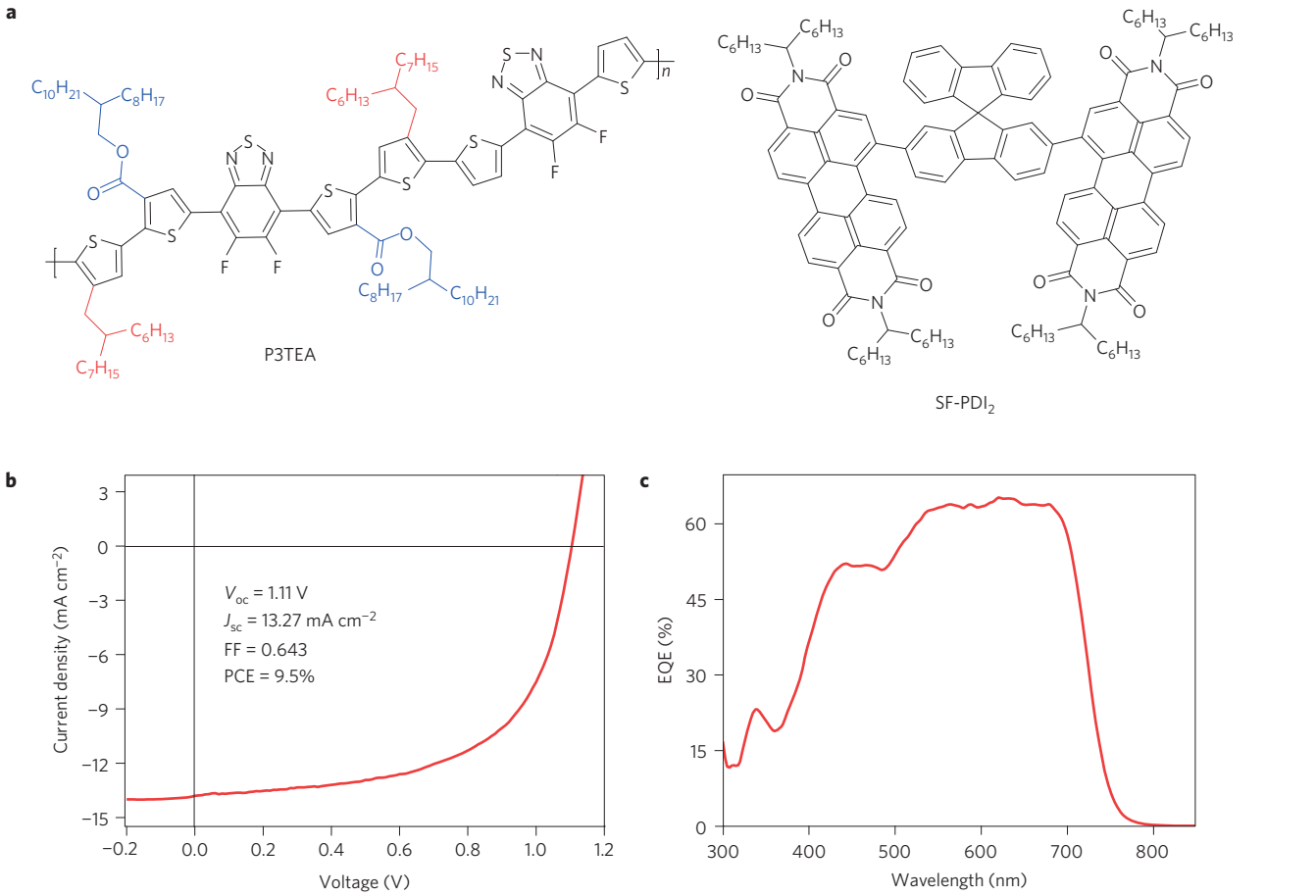

Figure 1 | Chemical structures and photovoltaic performance. a, Chemical structures of donor polymer P3TEA and SMA SF-PDI$_2$. **b**, The *J*–*V* curve of a blend A-based solar cell. Inset: device parameters of the blend A-based solar cell. **c**, The EQE curve of a blend A-based solar cell.

the highest reported for OSC blends so far, which suggests low non-radiative recombination loss of the blend. This leads to a high-efficiency (9.5%, Fig. 1b) non-fullerene OSC with a low voltage loss of 0.61 V (bandgap 1.72 eV, based on the crossing point between the absorption and emission spectra, Supplementary Fig. 1a, V_{oc} 1.11 V), maximum EQE of about 66% (Fig. 1c) and internal quantum efficiency (IQE) of nearly 90% (Supplementary Fig. 2). It appears that the negative trade-off between V_{oc} and J_{sc} is removed, which will have fundamental impact on the long-term development of OSCs.

Origins of small voltage loss

Based on the detailed balance theory (see Supplementary Note 1 for details), the voltage loss in solar cells (both organic and inorganic) (Supplementary Fig. 3) can be attributed to the three factors shown in equation (1)[8]:

$$\begin{aligned} q\Delta V &= E_{gap} - qV_{OC} \\ &= (E_{gap} - qV_{OC}^{SQ}) + (qV_{OC}^{SQ} - qV_{OC}^{rad}) + (qV_{OC}^{rad} - qV_{OC}) \\ &= (E_{gap} - qV_{OC}^{SQ}) + q\Delta V_{OC}^{rad,below\ gap} + q\Delta V_{OC}^{non\text{-}rad} \\ &= \Delta E_1 + \Delta E_2 + \Delta E_3 \end{aligned} \quad (1)$$

where q is the elementary charge, ΔV is the voltage loss, $\Delta V_{OC}^{rad,below\ gap}$ is the voltage loss of radiative recombination from the absorption below the bandgap, $\Delta V_{OC}^{non\text{-}rad}$ is the voltage loss of non-radiative recombination, V_{OC}^{rad} is the open-circuit voltage when there is only radiative recombination, and V_{OC}^{SQ} is the maximum voltage by the Shockley–Queisser limit, where the EQE is assumed to be step-wise (in other words, no EQE or absorption is present below the optical gap of the cell)[33].

The first term of the voltage loss in equation (1) ($E_{gap} - qV_{OC}^{SQ}$) is due to radiative recombination originating from the absorption above the bandgap. This loss is unavoidable for any type of solar cell and is typically between 0.25 and 0.30 eV (Table 1).

The second term in the equation ($q\Delta V_{OC}^{rad,below\ gap}$) is due to additional radiative recombination from the absorption below the bandgap. For inorganic and perovskite solar cells, which have steep absorption edges, $\Delta V_{OC}^{rad,below\ gap}$ is negligible (Table 1). However, this value is usually very high for OSCs, being 0.67 V for the benchmark P3HT:PCBM blend and 0.2 V for the highly efficient PTB7:PCBM blend (Table 1). The large $\Delta V_{OC}^{rad,below\ gap}$ in OSCs is due to the existence of CT states, which exhibit lower energy than the bandgap, thus resulting in a redshifted absorption. Therefore, to minimize $\Delta V_{OC}^{rad,below\ gap}$ in OSCs, the energy difference between the singlet exciton on the donor and/or acceptor and the CT states should be minimized. We measured the FTPS-EQE spectrum of blend A, and found that the absorption onset almost overlaps with that of the pure P3TEA in the normalized Fig. 2a. In other words, no sub-gap CT state absorption is observed. As a result, $\Delta V_{OC}^{rad,below\ gap}$ for blend A is estimated to be as low as 0.07 V (Table 1), which is significantly smaller than that observed in typical OSCs, and comparable to that in inorganic solar cells.

The third loss term ($q\Delta V_{OC}^{non\text{-}rad} = -kT\ \ln(EQE_{EL})$)[8] is due to non-radiative recombination, where k is the Boltzmann constant,

Table 1 | Comparison between blend A-based solar cell and other solar cells.

Type of solar cell	Materials	E_{gap}	qV_{OC}	$q\Delta V$	ΔE_1 $E_{gap} - qV_{OC}^{SQ}$	ΔE_2 $q\Delta V_{OC}^{rad,below\ gap}$	ΔE_3 $q\Delta V_{OC}^{non\text{-}rad}$
This work	Blend A	1.72	1.11	0.61	0.27	0.07	0.26
Inorganics	*c*-Si	1.12	0.68	0.44	0.25	0.01	0.18
	Perovskite (evaporated)	1.61	1.08	0.53	0.28	0.002	0.25
Traditional OSCs	P3HT:PCBM	1.93	0.58	1.35	0.30	0.67	0.38
	PTB7:PCBM	1.61	0.74	0.87	0.28	0.20	0.39

All values are in eV. The original data of the other four cells for comparison are taken from ref. 8.

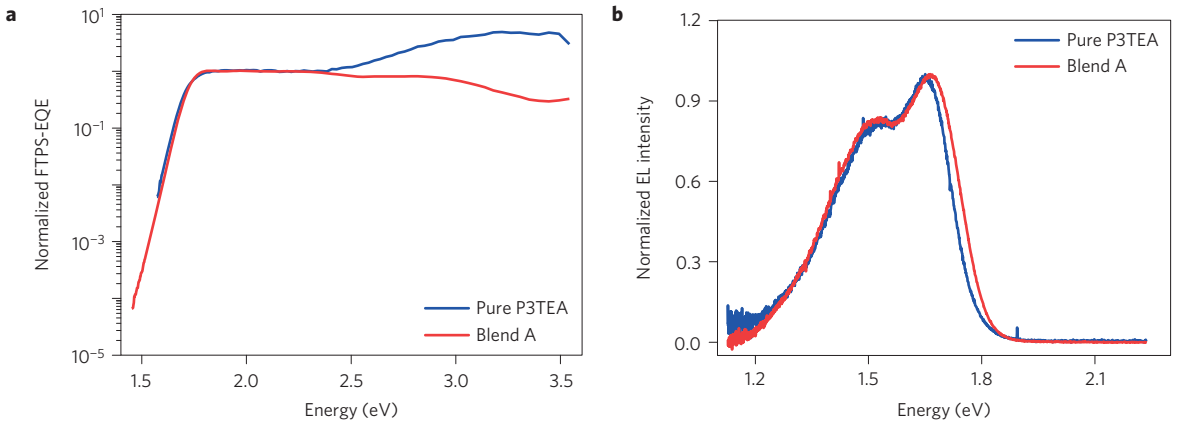

Figure 2 | Optical and electrical characterizations. a, Normalized FTPS-EQE spectra of pure P3TEA and blend A-based devices. **b**, Normalized EL curves of pure P3TEA and blend A-based devices.

T is temperature and EQE_{EL} is radiative quantum efficiency of the solar cell when charge carriers are injected into the device in the dark. To minimize this term, $q\Delta V_{OC}^{non\text{-}rad}$, it is important to maximize EQE_{EL}. At room temperature, $\Delta V_{OC}^{non\text{-}rad}$ increases by 60 mV when EQE_{EL} decreases by one order of magnitude[10]. For *c*-Si and perovskite solar cells, $\Delta V_{OC}^{non\text{-}rad}$ is about 0.25 V (Table 1). For organic solar cells, $\Delta V_{OC}^{non\text{-}rad}$ is much larger (0.38–0.44 V, Table 1) due to the very low EQE_{EL} of BHJ blends (typically on the order of 10^{-6}–10^{-8}). For the blend A-based solar cell, our measurement indicates a relatively high EQE_{EL} value of 0.5×10^{-4}, representing a voltage loss of 0.26 V. This value is much better than those for previously reported OSCs and similar to that for the high-quality evaporated perovskite devices. The value of V_{oc} calculated based on the EQE_{EL} values and equation (1) is in excellent agreement with that obtained in our experiment (Table 1). In addition, the EL spectrum of the blend A-based device is nearly identical to that of the pure polymer device (Fig. 2b), showing no emission from the CT states, which is consistent with the FTPS results shown in Fig. 2a. The emission from CT states typically exhibits a Gaussian distribution, while the emission of blend A clearly shows a vibronic shoulder similar to that observed for the pure polymer. These observations indicate that the EL emission of blend A is mainly from the polymer excitons, instead of CT states. As a result, the EQE_{EL} of blend A is also close to that of the pure P3TEA polymer.

Efficient charge separation with small driving force

As the FTPS-EQE and EL spectra of blend A are nearly identical to those of the pure polymer, the energy of the CT state should be very close to that of the singlet exciton, which means that the driving force for charge separation ($E_{gap} - E_{CT}$) is very small for blend A. With such a small driving force, the question arises whether the charge separation process in this blend is still fast and efficient. To investigate the charge separation kinetics of blend A, we performed femtosecond TAS to investigate charge generation dynamics in blend A. We used the pump excitation of 2.16 eV (575 nm) and maintain an initial photoexcitation density of $\sim 10^{16}$ cm^{-3} for all thin films. Figure 3a shows photoinduced absorption (PIA), resulting from the absorption of donor polymer singlet excitons, centred at ~0.9 eV, and a broad feature in the probe range of 1.1–1.5 eV due to the absorption of polarons in charge separated states. The assignments of the exciton and polaron PIA spectral features are consistent with earlier results of TAS in polymer blends[23,34,35].

We monitored the exciton absorption band (~0.9 eV) decay dynamics of the blend (Fig. 3b) and observed that the photoinduced electron transfer from donor to acceptor is fast, with a characteristic decay half-life of 3 ps. This electron transfer is an order of magnitude faster than the exciton lifetime (30 ps) of the donor polymer (Supplementary Fig. 4a), indicating the high efficiency of this electron transfer process for the blend. In addition, there is a significant population (~23%) of excitons that are already dissociated into charges within 100 fs (time resolution of our TAS set-up) (see Supplementary Fig. 5 for details). Furthermore, the PL quenching efficiency of blend A is about 87% (Supplementary Fig. 6), which is in agreement with the TAS data and indicates reasonably efficient exciton dissociation in the BHJ blend. These data demonstrate fast and efficient charge generation, despite the negligible driving force of blend A.

To better illustrate the influence of the driving force on charge generation dynamics, we compare the TAS data of blend A with the known PffBT4T-2DT:SF-PDI_2 blend (blend B) (Fig. 3b,d) that exhibits a significantly larger driving force (160 meV, Supplementary Fig. 1b,d). To estimate the driving force, the E_{gap} is determined from the crossing point between the normalized absorption and emission spectra, and the E_{CT} is determined from the sensitive FTPS-EQE measurements. Detailed data are shown in Supplementary Fig. 1.

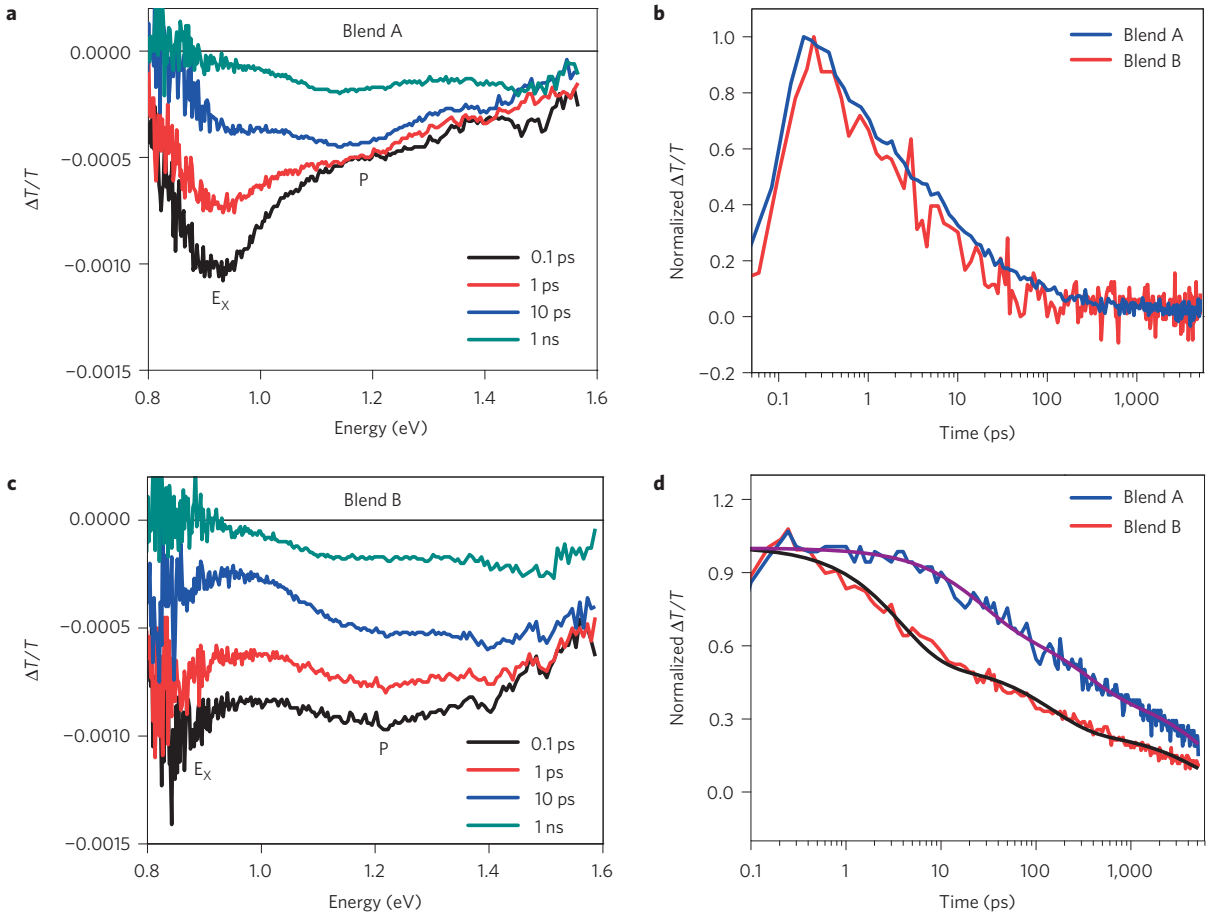

Figure 3 | Transient absorption data. a,**c**, Transient absorption spectra for blend A (**a**) and blend B (**c**) films. **b**,**d**, Time evolution of singlet exciton absorption (**b**) and polaron absorption (**d**) for blend A and blend B films; the pink and black solid lines are the fitting of absorption.

As shown in Fig. 3b, the decay dynamics of the exciton absorption band is very similar for the two blends, with a nearly identical characteristic decay half-lifetime of 3 ps, despite the differences in the driving force. We also monitored the charge separated polaron dynamics (∼1.2 eV) of both blended films (Fig. 3d). The decay time for polaron fits to a multiexponential with time constants; 24 ps (31%), 307 ps (29%) and >5 ns (40%) for blend A. For blend B, it is 3.8 ps (45%), 142 ps (26%) and >5 ns (29%). The large percentage of long-lived polarons suggests efficient charge generation and suppressed geminate recombination in the case of blend A. This conclusion is supported by the observation of nongeminate recombination at later delays in this blend from the intensity-dependent measurements (Supplementary Fig. 4b). This result indicates that the driving force may not be the most important factor governing the charge separation kinetics for our polymer:non-fullerene blends and that a small driving force does not have any negative impact on charge separation or recombination kinetics.

Influence of the driving force on EQE_{EL}

To further understand the relatively high EQE_{EL} of blend A-based cells, we study the influence of the driving force ($E_{gap} - E_{CT}$) on EQE_{EL} for four different blends during the charge transfer processes. These four blends exhibit similar morphology and they all have small domain size (Supplementary Figs 7–9).

$$EQE_{CT}(E) = \frac{f}{E\sqrt{4kT\pi\lambda}} \exp\left(\frac{-(E_{CT}+\lambda-E)^2}{4kT\pi\lambda}\right) \quad (2)$$

where λ is the reorganization energy associated with charge transfer absorption and f is a prefactor. We intentionally replace $SF\text{-}PDI_2$ with another SMA (named diPDI) that has a lower lowest unoccupied molecular orbital (LUMO) level than $SF\text{-}PDI_2$ or replace P3TEA with a polymer with a higher LUMO level (energy levels shown in Supplementary Fig. 10). The four materials in Supplementary Fig. 10 lead to four donor/acceptor combinations with different driving forces. For all the blends with larger driving force, the CT absorption is clearly visible in the FTPS-EQE spectra, and the E_{CT} can be determined by fitting the FTPS-EQE spectra (Supplementary Fig. 1). For blend A, as we show in Fig. 2a, the FTPS-EQE spectrum overlaps with that of the pure P3TEA. Therefore, we can safely conclude that driving force is very small, but it is difficult to determine an exact value. As the EQE_{EL} values of the blends have some slight dependence on applied voltage, we measured the EQE_{EL} of the four blends at different voltages and made a plot of EQE_{EL} versus voltage, as shown in Fig. 4. It is clear that the donor/acceptor blends with larger driving force values exhibit decreased EQE_{EL}, showing a good correlation between the EQE_{EL} and the driving force values (Fig. 4).

The trend in Fig. 4 indicates that an increasing number of polymer singlet excitons are populated with a decreasing driving force, resulting in higher EQE_{EL}. For the blends with larger driving force (for example, blend B; blend C, which is P3TEA:diPDI; and blend D, which is PffBT4T-2DT:diPDI), there is a greater probability for the recombination to occur through the CT states. It is well known that the EL emission from CT states is less efficient than that from the pure polymer excitons[15]. Therefore, the existence of sub-gap CT states results in an overall lower EQE_{EL}. In contrast,

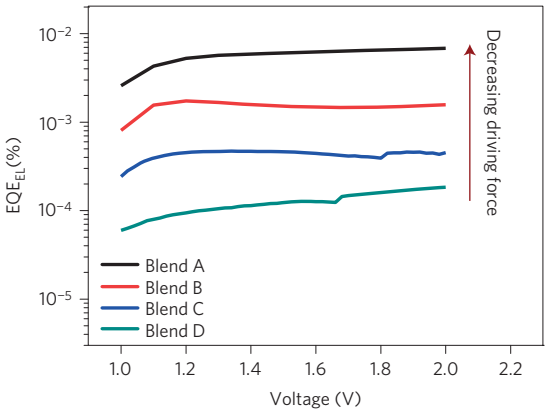

Figure 4 | EQE_{EL} spectra. EQE_{EL} of P3TEA:SF-PDI_2 (blend A), PffBT4T-2DT:SF-PDI_2 (blend B), P3TEA:diPDI (blend C) and PffBT4T-2DT:diPDI (blend D)-based solar cells at different voltages. The value of the driving force for blend A is negligible; for blend B it is 160 meV; for blend C it is 200 meV; and for blend D it is 370 meV.

for the case of blend A, as the driving force is small and there is no evident sub-gap CT states, the EL emission from the polymer exciton is maximized, which leads to a relatively high EQE_{EL}.

To better understand the influence of driving force on the EL properties of the blends, we further investigated the EL spectra of the blend C with relatively large driving force value (Supplementary Fig. 12a). Compared to pure P3TEA, the EL spectrum of blend C exhibits additional emission at energies lower than 1.6 eV. Gaussian fitting shows that the strong emission of the blend C at low energies is due to the existence of a Gaussian peak at 1.41 eV (Supplementary Fig. 12b), which can be attributed to the emission from CT states. To confirm that the additional emission from the blend C is due to the existence of a new state (that is, CT state), we compare the EL spectra of blend C (Supplementary Fig. 12c) with those of the pure P3TEA polymer (Supplementary Fig. 12d) at different injection currents. The low- and high-energy emission peaks of blend C have different dependences on the injection current, indicating that these peaks originate from different states. In contrast to blend C, the shape of the EL spectra of the pure P3TEA is independent of the injection currents, as both peaks are from the same states (polymer singlet excitons). This comparison further supports the low-energy emission peak of blend C being from a different state other than the polymer singlet exciton.

Impacts of the small driving force

For the four polymer:SMA blends presented in Fig. 4, the decrease of the driving force does not have any negative effects on the EQE and efficiencies of the devices. The device parameters of the four polymer:SMA OSCs in Supplementary Table 1 show that the highest V_{oc}, EQE, J_{sc} and efficiency values were simultaneously achieved for the material set (blend A) with the smallest driving force. It appears that the J_{sc} and EQE of these non-fullerene devices are not reversely interlocked with their V_{oc}, which is different from the trend observed for fullerene devices in Supplementary Fig. 13. Removing the trade-off between driving force and EQE would potentially allow non-fullerene OSCs to achieve maximal J_{sc} and V_{oc} at the same time, enabling a higher efficiency for OSCs.

Despite the small driving force between P3TEA and SF-PDI_2, blend A-based cells can still achieve high IQE values, which shows that the overall charge separation, transport and collection processes in these OSCs are highly efficient. This raises the important question how the charge separation can be efficient with a small driving force. Previous reports indicated that excitons in BHJ blends can delocalize at a length scale up to 10 nm (refs 36–38), which significantly reduces the Coulombic attraction between positive and negative charges, thus allowing efficient charge separation. Further steps of charge separations (from CT states to charge separated states) could be driven by the slight energetic difference between the amorphous and crystalline phases of the donor or acceptor[39]. The entropy increase associated with charge separation in a disordered manifold could also provide another possible source of driving force[40,41].

Although we have demonstrated fast and efficient charge separation for a non-fullerene OSC with a small driving force, our results should be relevant to fullerene OSCs as well. There have been extensive efforts in reducing the driving force for fullerene OSCs, with one recent example showing a small driving force, but the charge separation was relatively slow (100 ps) and PL quenching was about 66%[23]. If fullerene OSCs can achieve fast and efficient charge separation with a small driving force, the efficiencies of fullerene OSCs will probably increase beyond the present record (assuming the morphology and charge collection are all fully optimized). Compared to fullerene OSCs, tuning the energy offset between the donor and acceptor—and thus the driving force—in non-fullerene OSCs is probably more convenient, as we can readily change the energy levels of both the donor and acceptor materials. For fullerene OSCs, most high-efficiency cells are based on a specific fullerene, PCBM. Although hundreds of donor polymers have been reported, there are very limited examples (for example, PNOz4T) that exhibit small driving force yet still work efficiently.

Conclusion

To conclude, we report an efficient non-fullerene OSC with a negligible driving force, yet still exhibits efficient charge generation and separation. The FTPS-EQE and EL spectra of blend A have nearly identical shapes to those of the pure polymer, which indicates that the driving force for separation ($E_{gap} - E_{CT}$) is very small or nearly negligible. With such a small driving force, the blend A-based cells still exhibit fast charge separation with a characteristic half-lifetime of 3 ps. The PL quenching efficiency of blend A is also reasonably high (87%). This led to an efficient non-fullerene OSC with an IQE of nearly 90% and a PCE of 9.5%. By comparing two blends with different driving forces, we show that the small driving force does not have a negative impact on the charge separation or recombination dynamics. In addition, by examining four blends with different driving forces, we show that the EQE_{EL} of the blend decreases with increasing driving force, and that the blend with the smallest driving force exhibits the highest EQE_{EL} of about 0.5×10^{-4}, which is the highest value reported for OSC blends to date. This indicates that the extent of voltage loss from non-radiative recombination is the lowest for the blend with the smallest driving force. This provides a new approach to reduce voltage loss from non-radiative recombination in OSCs (by reducing driving force). As a result of the low driving force and relatively low voltage loss, the V_{oc} of blend A-based OSCs is high (1.11 V) despite a bandgap of 1.72 eV for the donor polymer. Our results show the critical role of small driving force and its impacts on charge separation, EL properties and non-radiative recombination loss. These insights should extend to both fullerene and non-fullerene OSCs. Our work presents the first example of efficient charge separation on a small driving force, which will have important fundamental implications on the development of more efficient OSCs.

Methods

Cyclic voltammetry measurement. Cyclic voltammetry was carried out on a CHI760E electrochemical workstation with three electrodes, using Ag/AgCl as the reference electrode, a Pt plate as the counter electrode, and a glassy carbon as the working electrode. 0.1 mol l^{-1} tetrabutylammonium hexafluorophosphate in anhydrous acetonitrile was used as the supporting electrolyte solution. Polymers and small molecules were drop-cast onto the electrode from chlorobenzene solutions (5 g l^{-1}) to form thin films. Potentials were referenced to the ferrocenium/ferrocene couple by using ferrocene as external standards in

acetonitrile solutions. All solutions were degassed by bubbling nitrogen for 20 min before measurement.

Atomic force microscopy characterization. Atomic force microscopy measurements were acquired by using a Scanning Probe Microscope-Dimension 3100 in tapping mode. All film samples were spincast on indium tin oxide (ITO)/ZnO substrates.

Ultraviolet–visible absorption. Ultraviolet–visible absorption spectra were acquired on a Perkin Elmer Lambda 20 UV/VIS Spectrophotometer. All film samples were spincast on ITO/ZnO substrates. PL spectra were measured on samples on ITO/ZnO substrates exposed to excitation by a laser beam using a Renishaw RM 3000 Micro- Raman/Photoluminescence system. All film samples were spincast on ITO/ZnO substrates.

GIWAXS characterization. GIWAXS measurements[42] were performed at beamline 7.3.3 at the Advanced Light Source (ALS). Samples were prepared on Si substrates using identical blend solutions as those used in devices. The 10 keV X-ray beam was incident at a grazing angle of 0.11°–0.15°, which maximized the scattering intensity from the samples. The scattered X-rays were detected using a Dectris Pilatus 2 M photon counting detector.

R-SoXS characterization. R-SoXS transmission measurements[43] were performed at beamline 11.0.1.2 at the ALS. Samples for R-SoXS measurements were prepared on a polystyrene sulfonate (PSS)-modified ITO substrate under the same conditions as those used for device fabrication, and then transferred by floating in water to a 1.5 × 1.5 mm, 100-nm-thick Si_3N_4 membrane supported by a 5 × 5 mm, 200-mm-thick Si frame (Norcada). Two-dimensional scattering patterns were collected on an in-vacuum charge-coupled device (CCD) camera (Princeton Instrument PI-MTE). The beam size at the sample is ∼100 mm by 200 mm. The composition variation (or relative domain purity) over the length scales probed can be extracted by integrating scattering profiles to yield the total scattering intensity. The purer the average domains are, the higher the total scattering intensity. Owing to a lack of absolute flux normalization, the absolute composition cannot be obtained only by R-SoXS.

EL measurement. EL spectra were detected using a light guide positioned close to the sample. The bias was applied on the devices using a Keithley 2400 SourceMeter. The detector was a Newton EM-CCD Si array detector at −60 °C with a Shamrock SR-303i spectrograph from Andor Tech.

EQE_{EL} measurement. EQE_{EL} values were obtained from an in-house-built system comprising a Hamamatsu silicon photodiode 1010B, a Keithley 2400 SourceMeter for supplying voltages and recording injected current, and a Keithley 485 picoammeter for measuring the emitted light intensity.

FTPS-EQE measurement. FTPS-EQE was measured using a Vertex 70 from Bruker Optics, equipped with a quartz tungsten halogen lamp, quartz beamsplitter and external detector option. A low-noise current amplifier (SR570) was used to amplify the photocurrent produced on illumination of the photovoltaic devices with light modulated by the Fourier transform infrared spectroscope (FTIR). The output voltage of the current amplifier was fed back into the external detector port of the FTIR, to be able to use the FTIR's software to collect the photocurrent spectrum.

Transient absorption measurement. Transient absorption data were collected using a TAS set-up. This set-up consists of a spectrometer (Ultrafast Helios system) and an amplified Ti:sapphire laser. The output of amplified Ti:sapphire laser provides 800 nm fundamental pulses at a 1 kHz repetition rate which were split into two optical beams to generate pump and probe pulses. One fundamental beam was used to generate pump beam using an optical parametric amplifier (OPA) system (Coherent Opera Solo). A white light/near-infrared probe was generated by focusing another fundamental beam into a flint glass. Pump and probe beams were focused on a sample and probe light was collected by a CCD device. The spectral detection region is 0.8–1.6 eV. The thin-film samples were encapsulated using ultraviolet curable glue before measurement. The instrument response function (IRF) was ∼100 fs full-width at half-maximum. The samples were excited at an excitation energy of 2.16 eV (575 nm) and the fractional change in transmission was detected in the probe range 0.8–1.6 eV at several time delays.

Solar cell fabrication and testing. Pre-patterned ITO-coated glass with a sheet resistance of ∼15 Ω per square was used as the substrate. It was cleaned by sequential sonication in soap deionized water, deionized water, acetone, and isopropanol for 30 min at each step. After ultraviolet/ozone treatment for 60 min, a ZnO electron transport layer was prepared by spin-coating at 5,000 r.p.m. from a ZnO precursor solution (diethyl zinc). Active layer solutions (D/A ratio 1:1.5, polymer concentration 9 mg ml^{-1}) were prepared in 1,2,4-trimethylbenzene (TMB) with 2.5% of 1,8-octanedithiol (ODT). To completely dissolve the polymer, the active layer solution should be stirred on a hotplate at 100 °C for at least 1 h. Before spin-coating, both the polymer solution and ITO substrate are preheated on a hotplate at approximately 90 °C. Active layers were spin-coated from the warm polymer solution on the preheated substrate in a N_2 glovebox at 1,500 r.p.m. to obtain thicknesses of ∼120 nm. The polymer:SMA blend films were then thermally annealed before being transferred to the vacuum chamber of a thermal evaporator inside the same glovebox. At a vacuum level of 3×10^{-6} torr, a thin layer (20 nm) of V_2O_5 was deposited as the anode interlayer, followed by deposition of 100 nm of Al as the top electrode. All cells were encapsulated using epoxy inside the glovebox. Device J–V characteristics were measured in forward direction under AM1.5G (100 mW cm^{-2}) at room temperature using a Newport solar simulator. The dwell time is 2 s and the speed is 0.8 V s^{-1}. We also conducted both forward and backward scans, which yielded identical results (Supplementary Fig. 15). The light intensity was calibrated using a standard Si diode (with KG5 filter, purchased from PV Measurement) to bring spectral mismatch to unity. J–V characteristics were recorded using a Keithley 236 SourceMeter unit. Typical cells have a device area of 5.9 mm^2, which is defined by a metal mask with an aperture aligned with the device area; certified cells have a area of 4.18 mm^2. EQE was characterized using a Newport EQE system equipped with a standard Si diode. Monochromatic light was generated from a Newport 300 W lamp source. EQE data from 300 to 850 nm is provided and the calculated J_{sc} (12.79 mA cm^{-2}) is comparable to that derived from J–V plots. In our experiments, over 30 devices have been tested, and the average efficiency is within 0.4% of our best value (Supplementary Table 3). We have also performed stability analysis, which indicates our organic solar cells are reasonably stable (Supplementary Fig. 16) (∼0.2–0.3% decrease in efficiency after two weeks).

Received 14 January 2016; accepted 24 May 2016; published 27 June 2016

References

1. Sariciftci, N. S., Smilowitz, L., Heeger, A. J. & Wudl, F. Photoinduced electron transfer from a conducting polymer to buckminsterfullerene. *Science* **258**, 1474–1476 (1992).
2. Yu, G., Gao, J., Hummelen, J. C., Wudl, F. & Heeger, A. J. Polymer photovoltaic cells: enhanced efficiencies via a network of internal donor-acceptor heterojunctions. *Science* **270**, 1789–1791 (1995).
3. Heeger, A. J. 25th anniversary article: bulk heterojunction solar cells: understanding the mechanism of operation. *Adv. Mater.* **26**, 10–27 (2014).
4. Guo, X. *et al.* Polymer solar cells with enhanced fill factors. *Nature Photon.* **7**, 825–833 (2013).
5. He, Z. *et al.* Enhanced power-conversion efficiency in polymer solar cells using an inverted device structure. *Nature Photon.* **6**, 593–597 (2012).
6. Liu, Y. *et al.* Aggregation and morphology control enables multiple cases of high-efficiency polymer solar cells. *Nature Commun.* **5**, 5293 (2014).
7. Vohra, V. *et al.* Efficient inverted polymer solar cells employing favourable molecular orientation. *Nature Photon.* **9**, 403–408 (2015).
8. Yao, J. *et al.* Quantifying losses in open-circuit voltage in solution-processable solar cells. *Phys. Rev. Appl.* **4**, 014020 (2015).
9. Vandewal, K., Tvingstedt, K., Gadisa, A., Inganäs, O. & Manca, J. V. Relating the open-circuit voltage to interface molecular properties of donor:acceptor bulk heterojunction solar cells. *Phys. Rev. B* **81**, 125204 (2010).
10. Vandewal, K., Tvingstedt, K., Gadisa, A., Inganas, O. & Manca, J. V. On the origin of the open-circuit voltage of polymer-fullerene solar cells. *Nature Mater.* **8**, 904–909 (2009).
11. Burke, T. M., Sweetnam, S., Vandewal, K. & McGehee, M. D. Beyond Langevin recombination: how equilibrium between free carriers and charge transfer states determines the open-circuit voltage of organic solar cells. *Adv. Energy Mater.* **5**, 1500123 (2015).
12. Tvingstedt, K. *et al.* Electroluminescence from charge transfer states in polymer solar cells. *J. Am. Chem. Soc.* **131**, 11819–11824 (2009).
13. Heumueller, T. *et al.* Disorder-induced open-circuit voltage losses in organic solar cells during photoinduced burn-in. *Adv. Energy Mater.* **5**, 1500111 (2015).
14. Vandewal, K. *et al.* Efficient charge generation by relaxed charge-transfer states at organic interfaces. *Nature Mater.* **13**, 63–68 (2014).
15. Scharber, M. C. *et al.* Design rules for donors in bulk-heterojunction solar cells—towards 10% energy-conversion efficiency. *Adv. Mater.* **18**, 789–794 (2006).
16. Li, W., Hendriks, K. H., Furlan, A., Wienk, M. M. & Janssen, R. A. High quantum efficiencies in polymer solar cells at energy losses below 0.6 eV. *J. Am. Chem. Soc.* **137**, 2231–2234 (2015).
17. Vandewal, K. *et al.* Quantification of quantum efficiency and energy losses in low bandgap polymer: fullerene solar cells with high open-circuit voltage. *Adv. Funct. Mater.* **22**, 3480–3490 (2012).

18. Wang, M. *et al.* High open circuit voltage in regioregular narrow band gap polymer solar cells. *J. Am. Chem. Soc.* **136**, 12576–12579 (2014).
19. Jung, J. W., Liu, F., Russell, T. P. & Jo, W. H. Semi-crystalline random conjugated copolymers with panchromatic absorption for highly efficient polymer solar cells. *Energy Environ. Sci.* **6**, 3301–3307 (2013).
20. Peng, Q. *et al.* Enhanced solar cell performance by replacing benzodithiophene with naphthodithiophene in diketopyrrolopyrrole-based copolymers. *Chem. Commun.* **48**, 11452–11454 (2012).
21. Ran, N. A. *et al.* Harvesting the full potential of photons with organic solar cells. *Adv. Mater.* **28**, 1482–1488 (2016).
22. Ma, Z., Wang, E., Vandewal, K., Andersson, M. R. & Zhang, F. Enhance performance of organic solar cells based on an isoindigo-based copolymer by balancing absorption and miscibility of electron acceptor. *Appl. Phys. Lett.* **99**, 143302 (2011).
23. Kawashima, K., Tamai, Y., Ohkita, H., Osaka, I. & Takimiya, K. High-efficiency polymer solar cells with small photon energy loss. *Nature Commun.* **6**, 10085 (2015).
24. Sauvé, G. & Fernando, R. Beyond fullerenes: designing alternative molecular electron acceptors for solution-processable bulk heterojunction organic photovoltaics. *J. Phys. Chem. Lett.* **6**, 3770–3780 (2015).
25. Zhan, X. *et al.* Rylene and related diimides for organic electronics. *Adv. Mater.* **23**, 268–284 (2011).
26. Zhong, Y. *et al.* Molecular helices as electron acceptors in high-performance bulk heterojunction solar cells. *Nature Commun.* **6**, 8242 (2015).
27. Chen, Z. *et al.* Low band-gap conjugated polymers with strong interchain aggregation and very high hole mobility towards highly efficient thick-film polymer solar cells. *Adv. Mater.* **26**, 2586–2591 (2014).
28. Mao, Z. *et al.* Azadipyrromethene-based Zn(II) complexes as nonplanar conjugated electron acceptors for organic photovoltaics. *Adv. Mater.* **26**, 6290–6294 (2014).
29. Zhao, J. *et al.* High-efficiency non-fullerene organic solar cells enabled by a difluorobenzothiadiazole-based donor polymer combined with a properly matched small molecule acceptor. *Energy Environ. Sci.* **8**, 520–525 (2015).
30. Lin, H. *et al.* High-performance non-fullerene polymer solar cells based on a pair of donor–acceptor materials with complementary absorption properties. *Adv. Mater.* **27**, 7299–7304 (2015).
31. Sun, D. *et al.* Non-fullerene-acceptor-based bulk-heterojunction organic solar cells with efficiency over 7%. *J. Am. Chem. Soc.* **137**, 11156–11162 (2015).
32. Lin, Y. *et al.* An electron acceptor challenging fullerenes for efficient polymer solar cells. *Adv. Mater.* **27**, 1170–1174 (2015).
33. Shockley, W. & Queisser, H. J. Detailed balance limit of efficiency of p–n junction solar cells. *J. Appl. Phys.* **32**, 510–519 (1961).
34. Shivanna, R. *et al.* Charge generation and transport in efficient organic bulk heterojunction solar cells with a perylene acceptor. *Energy Environ. Sci.* **7**, 435–441 (2014).
35. Deshmukh, K. D. *et al.* Performance, morphology and photophysics of high open-circuit voltage, low band gap all-polymer solar cells. *Energy Environ. Sci.* **8**, 332–342 (2015).
36. Chen, K., Barker, A. J., Reish, M. E., Gordon, K. C. & Hodgkiss, J. M. Broadband ultrafast photoluminescence spectroscopy resolves charge photogeneration via delocalized hot excitons in polymer: fullerene photovoltaic blends. *J. Am. Chem. Soc.* **135**, 18502–18512 (2013).
37. Gélinas, S. *et al.* Ultrafast long-range charge separation in organic semiconductor photovoltaic diodes. *Science* **343**, 512–516 (2014).
38. Jamieson, F. C. *et al.* Fullerene crystallisation as a key driver of charge separation in polymer/fullerene bulk heterojunction solar cells. *Chem. Sci.* **3**, 485–492 (2012).
39. Sweetnam, S. *et al.* Characterization of the polymer energy landscape in polymer: fullerene bulk heterojunctions with pure and mixed phases. *J. Am. Chem. Soc.* **136**, 14078–14088 (2014).
40. Gregg, B. A. Entropy of charge separation in organic photovoltaic cells: the benefit of higher dimensionality. *J. Phys. Chem. Lett.* **2**, 3013–3015 (2011).
41. van Eersel, H., Janssen, R. A. J. & Kemerink, M. Mechanism for efficient photoinduced charge separation at disordered organic heterointerfaces. *Adv. Funct. Mater.* **22**, 2700–2708 (2012).
42. Hexemer, A. *et al.* A SAXS/WAXS/GISAXS beamline with multilayer monochromator. *J. Phys. Conf. Ser.* **247**, 012007 (2010).
43. Gann, E. *et al.* Soft X-ray scattering facility at the Advanced Light Source with real-time data processing and analysis. *Rev. Sci. Instrum.* **83**, 045110 (2012).

Acknowledgements

The work described in this paper was partially supported by the National Basic Research Program of China (973 Program; 2013CB834701 and 2014CB643501), the Hong Kong Research Grants Council (T23–407/13 N, N_HKUST623/13, and 606012), HK JEBN Limited, and the National Science Foundation of China (nos 21374090 and 51361165301). X-ray characterization by NCSU was supported by the Office of Naval Research (award nos N000141410531 and N000141512322). Ultrafast spectroscopy work at NCSU was supported by Office of Naval Research (award no N000141310526 P00002). X-ray data were acquired at beamline 7.3.3 and 11.0.1.2 at the Advanced Light Source, which was supported by the Director, Office of Science, Office of Basic Energy Sciences, of the US Department of Energy under contract no. DE-AC02–05CH11231. The research at Linköping is financially supported by the Swedish Research Councils (VR, grant no. 330-2014-6433 and FORMAS, grant no. 942-2015-1253), the Swedish Government Strategic Research Area in Materials Science on Functional Materials at Linköping University (faculty grant SFO-Mat-LiU # 2009-00971), the European Commission Marie Skłodowska-Curie actions (grant nos 691210 and INCA 600398), and a Wallenberg Scholar grant to O.I.

Author contributions

J.L. and S.C. contributed equally to this work. J.L. synthesized the polymer and carried out the cyclic voltammetry, atomic force microscopy, transmission electron microscopy and PL characterizations; S.C. fabricated the solar cell devices and carried out ultraviolet measurements; D.Q. performed the FTPS and EL experiments supervised by F.G.; G.Y. analysed the GIWAXS and R-SoXS data supervised by W.M.; B.G. performed the TAS experiments supervised by K.G.; J.B. carried out the IQE measurement; J.Z., F.Z., H.A. and O.I. helped in the data interpretation. H.Y., F.G., J.L., S.C. and J.Z. wrote the manuscript; H.Y. conceived and directed the project; all authors discussed the results and commented on the final manuscript.

Additional information

Supplementary information is available online. Reprints and permissions information is available online at www.nature.com/reprints. Correspondence and requests for materials should be addressed to K.G., F.G. or H.Y.

Competing interests

The authors declare no competing financial interests.